Saturation effect in the optical response of Ag-nanoparticle fractal aggregates

Andrei K. Buin,[1,*] Peter F. de Châtel,[1] Heinz Nakotte,[1] Vladimir P. Drachev,[2] and Vladimir M. Shalaev[2]
[1]*Physics Department, New Mexico State University, Las Cruces, New Mexico 88003, USA*
[2]*School of Electrical and Computer Engineering, Purdue University, West Lafayette, Indiana 47907, USA*
(Received 11 May 2005; revised manuscript received 28 October 2005; published 31 January 2006)

The enhancement and extinction spectra for fractal aggregates consisting of monodisperse nanosized silver particles are studied theoretically. We find the iterative solution to the coupled-dipole equations in the quasistatic approximation, taking into account a contribution of the nonlinear susceptibility $\chi^{(3)}$ to the intensity-dependent dielectric function. Using a modified version of Broyden's method, the self-consistent problem was solved and convergence of the solutions for the dipole moments was achieved, even in the case of "weak" hysteretic behavior. The nonlinearity partly suppresses the giant enhancement of the local electrical fields obtained previously within the linear theory. Our calculations for fractal aggregates consisting of silver particles with radii of 3 and 5 nm show strong saturation effects of the optical transitions, which, in the case of 5-nm particles, are accompanied by hysteretic effects.

DOI: 10.1103/PhysRevB.73.035438 PACS number(s): 78.70.−g, 05.45.Df, 78.67.Bf

I. INTRODUCTION

Fractal aggregates of small, nanometer-sized metallic particles have some stunning differences with the optical properties of both colloidal solutions of isolated particles and close-packed crystal-like structures. In the latter cases, the optical absorption is limited to a narrow frequency range, centered at the surface-plasmon frequency in colloids and limited to the band of frequencies of propagating modes in crystals. In contrast, the absorption spectrum of fractal aggregates extends over a wide range of frequencies, including the infrared. Concomitantly, the internal field in some of the metallic particles is enhanced, with respect to the incident field, $\mathbf{E}_0=\mathbf{E}^0_{\max}e^{i\omega t}$ by several orders of magnitude. This enhancement is caused by interparticle interaction and is related to resonant states extending over a limited range, reflected in huge enhancements of spatially limited *hot spots*.

The ability of small metal particles and aggregates to enhance local fields strongly influences their optical properties, including ultrafast nonlinear response and surface-enhanced Raman spectroscopy (SERS).[1–6] Such properties have generated some interest in using nanoparticle aggregates for single-molecule sensing[7–9] as well as for femtosecond studies of energy localization[10] at the nanoscale. In nature, aggregates of particles may form fractal structures, which can be described as a system of dimension less than 3.[11,12] Large ensembles of small aggregates can be described using the concept of fractal dimension of these aggregates as a statistically defined property.[12] It should be noted that the aggregate size is crucial to the nonlocal nonlinear response (nonlinear optical activity).[13,14]

Previous studies have shown that interparticle interaction can lead to enhancements of the local field intensity by several orders of magnitude (more than 10^5).[9] The local intensities may be very high so that the particle dipole moments can be expected to be nonlinear. Hence, the nonlinear contributions to the polarizability of the metal particle can be important even for linear processes such as SERS or femtosecond light manipulation at the nanoscale.

Various theoretical methods have been applied to study the properties of fractal aggregates consisting of nanosized metal particles. Some of the earliest attempts used a theory based on Mie scattering and extinction for a spherical particle and subsequent solution of an electromagnetic boundary problem.[15,16] While such an approach can be used to determine near- and far-field features beyond the dipole approximation, it is not clear how to introduce nonlinear corrections. A second approach is the finite-difference time-domain, which can be applied to the problem of linear response of a small group of metal particles,[17] and it was used also in a nonlinear case for particles with a nonlinear susceptibility similar to the bulk one.[18] In our system, this is not the case; i.e., the nonlinear susceptibility of the Ag nanoparticles considered here differs substantially from the one of bulk silver. A third approach may be to directly solve Maxwell equations using the discrete dipole approximation,[19] although this is limited to aggregates with relatively small numbers of particles. For sufficiently small particles, coupled-dipole equations (CDEs) that treat each particle as a dipole can be employed.[20] This approach is used in our paper. A major advantage of the CDE method is that the nonlinear dipole moment of a particle as a whole can be used to determine frequency and size dependencies of the optical properties.

The enhancement of the incident electric field in aggregates has two distinguishable sources: the internal field of the particle and the dipole interactions. The internal field in the metallic particles, the "monomers," acquires a significant contribution due to the inhomogeneous charge distribution inside the particle. Throughout the paper, we will use esu units and assume that the particles are spherical. The particles can then be fully characterized by the dielectric function of the constituent metal, and the internal field is given by[21]

$$\mathbf{E}_i=\frac{3\varepsilon_h}{\varepsilon_m+2\varepsilon_h}\mathbf{E}^0=f(\omega)\mathbf{E}^0. \quad (1)$$

Here, ε_h and ε_m are the linear dielectric functions of the host and the metal, respectively, and $f(\omega)$ will be referred to as

the local field enhancement factor. Inside the sphere of radius R, the field is uniform; outside, it is identical with the field of a point-like dipole

$$\mathbf{d} = R^2 \varepsilon_h \frac{\varepsilon_m - \varepsilon_h}{\varepsilon_m + 2\varepsilon_h} \mathbf{E}^0 = \alpha \varepsilon_h \mathbf{E}^0 \tag{2}$$

situated at the center of the sphere. Equation (2) implicitly defines the polarizability α.

The radiation field of the oscillating dipole moment of a monomer extends to large distances and dominates the interaction with other monomers within the aggregate. The mean-field description of the resulting collective effects, which is used in the electrodynamics of continuous media, breaks down when the monomers form a fractal cluster.[22] Therefore, it is necessary in such cases to deal with the interaction between the induced dipole moments individually. This leads to the coupled-dipole equations[19]

$$\mathbf{d}_i = \alpha \left\{ \varepsilon_h \mathbf{E}^0 e^{i\mathbf{k}\cdot\mathbf{r}_{ij}} + \sum_{\substack{j \\ j\neq i}} [(3\hat{\mathbf{r}}_{ij}(\hat{\mathbf{r}}_{ij}\cdot\mathbf{d}_j) - \mathbf{d}_j)(1 - ikr_{ij}) - (kr_{ij})^2 \hat{\mathbf{r}}_{ij} \times (\hat{\mathbf{r}}_{ij} \times \mathbf{d}_j)] \frac{e^{ikr_{ij}}}{r_{ij}^3} \right\}, \tag{3}$$

where $\mathbf{d}_i$ is the dipole moment induced on particle i, $\mathbf{r}_{ij} = \mathbf{r}_i - \mathbf{r}_j$, and a hat indicates a unit vector. If the wavelength of the incident radiation substantially exceeds the size of the entire aggregate, i.e., $kr_{ij} \ll 1$, the phase factors in Eq. (3) can be omitted and only the near field, $[3\hat{\mathbf{r}}_{ij}(\hat{\mathbf{r}}_{ij}\cdot\mathbf{d}_j) - \mathbf{d}_j]/r_{ij}^3$ needs to be considered. The resulting CDE takes the form

$$d_{i,\alpha} = \alpha \left[\varepsilon_h E_\alpha^0 + \sum_{\substack{j \\ j\neq i}} \sum_{\beta} W_{ij,\alpha\beta} d_{j,\beta} \right], \tag{4}$$

where the Greek indices indicate Cartesian components and

$$W_{ij,\alpha\beta} = (3\hat{r}_{ij,\alpha}\hat{r}_{ij,\beta} - \delta_{\alpha\beta})/r_{ij}^3. \tag{5}$$

The near field being identical to the field of a static dipole, the CDE of Eq. (4) is said to be in the quasistatic approximation, in which the time dependence of $\mathbf{E}^0$ is implied, but its $\mathbf{r}$ dependence is neglected because the wavelength of the incident field is typically two orders of magnitude larger than the size of the particles. However, as it was shown above, the quasistatic approximation can be fully justified only if the wavelength is larger than the size of the entire aggregate. The numerical calculations reported in the present paper concern fractal aggregates with linear dimensions up to 300 nm, which are not negligible compared to the wavelengths treated. To verify the validity of the quasistatic approximation, we have solved the CDE using the exact expression [Eq. (3)] for the radiation field; i.e., setting

$$W_{ij,\alpha\beta} = [(3(1 - ikr_{ij}) - (kr_{ij})^2)\hat{r}_{ij}\hat{r}_{ij} - ((1 - kr_{ij}) - (kr_{ij})^2)\delta_{\alpha\beta}] e^{ikr_{ij}}/r_{ij}^3. \tag{6}$$

The outcome of these calculations did not differ discernibly from the results obtained in the quasistatic approximation, once averaging over the orientation of the wave vector $\mathbf{k}$ and over the polarization of the incoming radiation field took place. There are some notable differences between the results found with the interaction matrices (5) and (6) if one looks at the enhancement of the dipole moments at particular sites for particular orientations of the field; these will be discussed in some detail in Sec. V.

A further concern about the approximations we have used is that the CDE does not give an exact description of the response of an aggregate, even if the exact interaction matrix (6) is used. While the incoming field generates only dipole moments in spherical particles, the field generated by these dipoles at neighboring sites is inhomogeneous on the scale of the particles, and it will result in multipole moments of higher orders. The effect of those was not explicitly included here because of complexity of nonlinear problem in this case. Similar to previous approaches,[4,23] to mimic the effect of multipole interactions, we allow the spheres to overlap, which, for fractal dimensionality 1.78, enhances the nearest-neighbor coupling by a factor of 1.91. Markel *et al.*[24] have shown that the introduction of overlapping spheres does not fully describe the actual contributions from the higher-order multipole moments. In particular, their calculations, which include multipoles up to $\ell = 64$, show a marked peak in the density of eigenmodes at the resonance frequency of the monomers, which is not seen in the dipole approximation, no matter what radius is chosen for the overlapping spheres. On the other hand, the averaged extinction calculated in the dipole approximation with one particular value of the radius comes very close to the result obtained with proper inclusion of the higher multipoles. In fact, the self-consistent solutions of the coupled-dipole equations found in the overlapping-spheres approximation reproduce well the experiments.[25] Most published works on fractal aggregates optics are limited to this approximation. Thus, it is reasonable to adopt the approach of overlapping spheres here and define the new features coming from the coupled nonlinear dipoles relative to the linear dipoles.

Much of this earlier work, in particular the results in Ref. 25, implied the existence of *hot spots*, where intensity enhancement factor as large as 10^5, were found in the linear approximation of the CDE. Considering possibility of a nonlinear relation between induced moments and the local field, one may wonder up to what incident light intensities the linear approximation remains valid. Clearly, there must be a limit of validity, because the Coulomb self-energy of the charge distribution scales with the square of the incident field and at one point will lead to saturation effects. Within the quasistatic approximation such effects can be treated in terms of higher-order response functions.[26–28]

To date, the problem of interparticle interactions in aggregates has been treated under the assumption of equal polarizability for all particles involved.[2] In general, only the linear contribution to the particle dipole moment was included for calculating the local field enhancement factor and related properties, even if the nonlinear optical response of aggregates was explored.

In this paper, we tackle the problem of interparticle interaction in aggregates with intensity-dependent and site-specific polarizability of particles and its effect on the en-

hancement factor and extinction spectra. In our approach, we invoke the scenario of saturation effects of optical transitions for conduction electrons resulting in the nonlinear dipole moments of metal particles. To calculate the linear and cubic nonlinear contributions to the dipole moment, we employed the analytical solution obtained by S.G. Rautian for linear and cubic nonlinear terms of the dipole moment.[26] Rautian's approach reproduces the Drude formula for the linear term in contrast to an approach proposed by Hache *et al.*[27] Rautian's approach also reproduces the classical result for the size-dependent linear term of the dielectric function.[1] In a recent paper,[28] we have shown that Rautian's model reproduces the experimentally observed values and size dependence of the nonlinear term for nanosized Ag particles by Uchida *et al.*[29] Here, we extend our studies to fractal aggregates consisting of nanosized particles. At high incident intensities, the polarizability of distinct particles is expected to be different due to the inhomogeneous local field distribution throughout the aggregate.

We explore the effect of the third-order polarization of metallic spheres by means of numerical calculations for various particle sizes. As mentioned above, for the linear and third-order dielectric constants, we rely on the seminal paper by Rautian,[26] and its main findings will be outlined in Sec. II. Section III describes the nonlinear coupled dipole equations and our numerical procedures. The convergence criteria and our approach will be outlined in Sec. IV. Our results will be presented and discussed in Sec. V, followed by conclusions in Sec. VI.

II. THIRD-ORDER POLARIZABILITY

The linear polarizability α can easily be calculated from Eq. (2), if the particle size and the linear dielectric functions are known. Third-order susceptibilities of various metals are less easily available and the determination of their effect on the dipole moment of an embedded small particle is not straightforward. In the microscopic theory of the polarizability of a small metal particle the bulk properties of the metal are not necessarily relevant for nanosized particles. In particular, the density of states may cease to be meaningful, and one has to deal with discrete energy eigenvalues. A discrete spectrum of electron states has indeed been observed experimentally in two-photon excited luminescence spectra for nanosized Ag particles.[30] Rautian[26] calculated the dipole moment induced in an electron gas enclosed in a spherical potential well of infinite depth. This simplified potential enabled the exact analytical treatment of individual eigenstates. The drawback of this model is that the properties of the surrounding medium (e.g., ε_h) cannot have any influence through the infinite potential barrier and the "spilling out" of electron wave functions cannot be studied; thus, the model neglects any effect of a surrounding medium or the depolarizing field. On the other hand, the time dependence of the perturbation is treated in a systematic way and it leads to the proper frequency dependence of the dipole moment. However, the introduction of Rautian's results into the formalism outlined above is not trivial. In particular, the electric field introduced in the quantum-mechanical calculation is obviously the internal field, which, however, contains ε_m [cf. Eq. (1)], whose doubtful relevance motivated the quantum-mechanical calculation at the outset.

Following the conventional approach,[31] we introduce the third-order polarizability in the effective dielectric constant, which depends on the intensity inside the particle, $I_p=|E_p|^2$:

$$\varepsilon_m = \varepsilon_m^1 + 12\pi\chi^{(3)}I_p. \tag{7}$$

We shall use Rautian's result assuming a linearly polarized field, which gives

$$\varepsilon_m^1 = \varepsilon_d - \left(\frac{\omega_p}{\omega}\right)^2\left\{F_1\left[1 - i\frac{2\Gamma_2}{\omega}\right] - ig_1\frac{\delta_F}{\hbar\omega}\right\}; \tag{8}$$

$$\chi^{(3)} = \frac{1}{30\pi}\left(\frac{\omega_p}{\omega}\right)^2\left(\frac{eR}{\hbar\omega}\right)^2\frac{\Gamma_2}{\Gamma_1}\left\{F_3\left[1 - i\frac{2\Gamma_2}{\omega}\right] - ig_3\left(\frac{g_F}{\hbar\omega}\right)^5\left(\frac{\omega}{2\Gamma_2}\right)^2\right\}. \tag{9}$$

Here, ε_d is the interband contribution to the linear dielectric function, $\omega_p=\sqrt{4\pi ne^2/m_e}$ is the plasma frequency, Γ_1 and Γ_2 are phenomenological longitudinal and transverse relaxation constants, $\delta_F=2\sqrt{E_FE_0}$, where E_F is the Fermi energy and $E_0=\hbar^2/2m_eR^2$ is the measure of the spacing of energy eigenvalues in the infinite potential well. The relaxation constants were chosen based on the criteria discussed in our previous paper,[28] and we used $\Gamma_1=5$ cm^{-1} and $\Gamma_2=60$ cm^{-1}, which are consistent with the reported range of experimental data. The parameters F_1 and F_3 result from the summation of nonresonant terms close to E_F. It was pointed out already by Rautian, that these two parameters are wavelength independent and relatively insensitive to the particle size. For our case, $F_1 \approx 0.95$ and $F_3 \approx 0.30$.[28] The parameters g_1 and g_3 result from the integration over all resonant states. Unlike the case of single particles, where the resonance half-width is limited to a relatively narrow wavelength range, we are faced here with the fact that in a fractal aggregate, a very broad spectral range needs to be considered. Thus, we can no longer assume that g_1 and g_3 remain approximately constant for all wavelengths of interest,[32] and we computed g_1 and g_3 as functions of the wavelength using the following integrals:

$$g_1(\omega) = 0.765\frac{E_F}{\hbar\omega}\int_{1-\hbar\omega/E_F}^{1} x^{3/2}\left(x + \frac{\hbar\omega}{E_F}\right)^{1/2} dx,$$

$$g_3(\omega) = 0.765\frac{E_F}{\hbar\omega}\int_{1-\hbar\omega/E_F}^{1} x^{5/2}\left(x + \frac{\hbar\omega}{E_F}\right)^{3/2} dx. \tag{10}$$

The results of the integration are shown in Fig. 1.

III. NONLINEAR CDE AND NUMERICAL PROCEDURE

With the introduction of the intensity-dependent dielectric function, the CDEs become more bothersome, for two reasons.

First, in Eq. (4), the polarizability becomes i dependent, because ε_m in Eq. (7) is determined by $I_{i,p}=|f_i(\omega)|^2I_{i,local}$, representing the enhanced intensity in particle $i=\{1,\ldots,N\}$. Here,

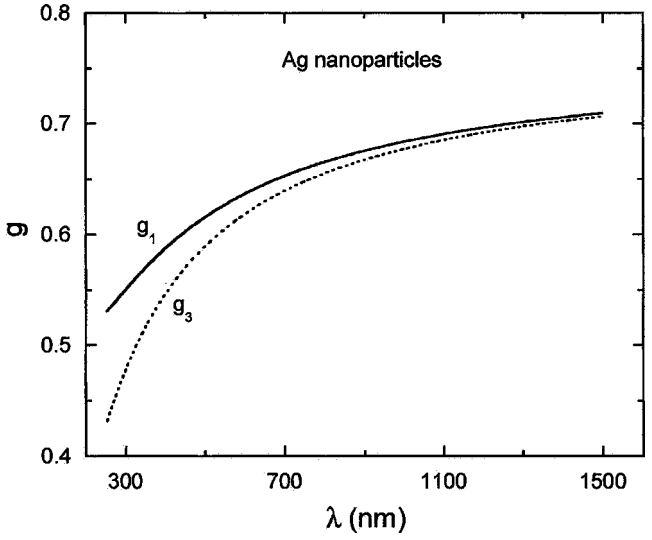

FIG. 1. Wavelength dependence of g_1 and g_3 for Ag particles.

$$I_{i,local} = \frac{|d_i|^2}{\varepsilon_h^2 |\alpha_i|^2} \tag{11}$$

is the combined intensity in particle i, which is due to the incident field plus the field emanating from all other particles.

Second, the enhancement factor $f_i(\omega)$ itself also depends on i through ε_m:

$$f_i(\omega) = \frac{3\varepsilon_h}{\varepsilon_m^1 + 12\pi\chi^{(3)}|f_i(\omega)|^2 I_{i,local} + 2\varepsilon_h}. \tag{12}$$

It was shown in Ref. 28 that Eq. (11) can be reduced to an algebraic equation, third-order in $|f_i(\omega)|^2$, with coefficients depending on ε_m^1, $\chi^{(3)}$, and $I_{i,local}$. This equation can be solved numerically. In other words, if the dielectric functions of the metal are known, a function $|f(\omega)|^2 = F(I_{local})$ can be deduced. The $|f_i(\omega)|^2$ determined in this way can be substituted into Eq. (12) and the site-dependent polarizability follows from a slight rearrangement of Eq. (2):

$$\alpha_i = R^3[1 - f_i(\omega)]. \tag{13}$$

With that, we can rewrite the CDE [Eq. (4)] in the more convenient form

$$d_{i,\alpha} = R^3[1 - f_i(\omega)]\left[\varepsilon_h E_\alpha^0 + \sum_{\substack{j \\ j \neq i}} W_{ij,\alpha\beta} d_{j,\beta}\right], \tag{14}$$

and the dipolar interaction matrix $W_{ij,\alpha\beta}$ is independent of ε_m and ε_h.[33]

Thus, we are faced with a many-body problem with position-dependent and thus nonconstant coupling parameters [Eqs. (11)–(14)], which is indeed a very challenging theoretical problem. Furthermore, we are clearly confronted with a self-consistency problem, which can be represented by the loop shown in Fig. 2. For the iterative procedure chosen in our approach, this means that the dipole moments in the kth iteration, $d_{i,\alpha}^{(k)}$, and thus the intensities inside the particles, $I_p^{(k)}$, depend on the $(k-1)$th iteration of $\alpha^{(k-1)}$. This is emphasized again in the flow chart shown in Fig. 3.

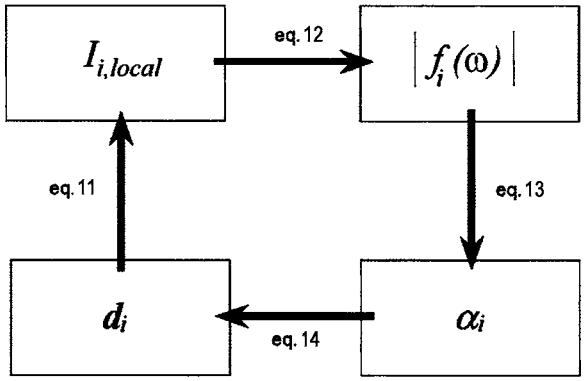

FIG. 2. Relationship between enhancement factor, local field intensity, absorption, and electric dipole moment.

At the beginning of the iterative process, we start with the assumption that the fields are the same on each monomer, and this gives the zeroth approximation of our self-consistent field cycle. The most demanding step in Fig. 2 is the solution of Eq. (14). This is the operation that takes the iterative process to the next level. To find the solution, we write the CDE in the matrix form:

$$(\hat{Z}^{(k-1)} - \hat{W}) \cdot \bar{\mathbf{d}}^{(k)} = \bar{\mathbf{E}}^0. \tag{15}$$

Here, $\hat{Z}^{(k-1)} = \delta_{ij}\delta_{\alpha\beta}(1/\alpha_i^{(k-1)})$ and $\hat{W} = W_{ij,\alpha\beta}$ are $3N \times 3N$ matrices, $\bar{\mathbf{d}}^{(k)} = d_{i\alpha}^{(k)}$ and $\bar{\mathbf{E}}^0 = \delta_{ij} E_\alpha^0$ are $3N$-dimensional vec-

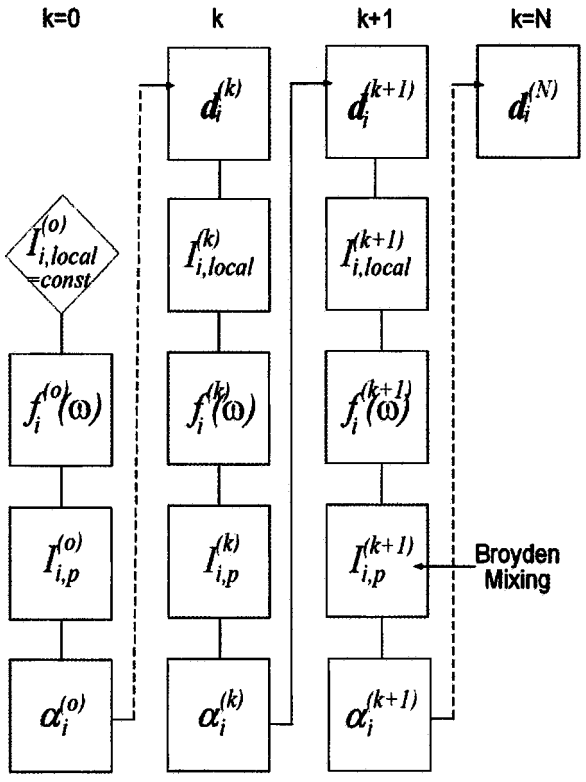

FIG. 3. Flow chart of the numerical procedure. The Broyden mixing is used at the level indicated.

tors and $\alpha_i^{(k-1)}=R^3[1-f_i^{(k-1)}(\omega)]$. As the matrix $\hat{Z}$ is not Hermitian, the solution cannot be found easily in terms of the eigenfunctions of the aggregate, so that the LU expansion was used instead:[34]

$$A = (\hat{Z}^{(k-1)} - \hat{W}) \equiv LU, \tag{16}$$

where L is the lower triangular matrix, and U is the upper triangular matrix. If the LU decomposition can be found, then obtaining the solution is relatively straightforward.

The polarizability $\alpha_i^{(k)}$ of particle i was computed through an iterative procedure and the superscript k indicates the result for the kth iteration:

$$\alpha_i^k = R^3 \frac{\varepsilon_m^1 + 12\pi\chi^{(3)} I_{i,p}^{(k)} - \varepsilon_h}{\varepsilon_m^1 + 12\pi\chi^{(3)} I_{i,p}^{(k)} + 2\varepsilon_h}, \tag{17}$$

where ε_m^1 and $\chi^{(3)}$ are the linear and nonlinear dielectric functions of the metal monomer, respectively, the latter derived from the nonlinear susceptibility of the monomer.[26] The intensity $I_{i,p}^{(k)}$ inside the ith particle at kth iteration can be derived from the enhancement factor $f_i^{(k)}(\omega)$ of one single monomer:

$$|f_i^{(k)}(\omega)|^2 = \frac{|E_{i,p}^{(k)}|^2}{|E_{i,local}^{(k)}|^2} = \frac{I_{i,p}^{(k)}}{I_{i,local}^{(k)}}. \tag{18}$$

The local intensity, $I_{i,local}^k$ of the ith particle at kth iteration is given by

$$I_{i,local}^k = \frac{d_{i,\alpha}^{(k)} (d_{i,\alpha}^{(k)})^*}{\varepsilon_h^2 |\alpha_i^{(k-1)}|^2}, \tag{19}$$

where summation over the repeated subscript α is implied.

The resulting local intensities per particle determine the average enhancement of the local field intensity of the fractal aggregate at the kth iteration

$$G^{(k)} = \frac{\langle |E_{i,local}^{(k)}|^2 \rangle}{|E_0|^2}. \tag{20}$$

Solving the third-order algebraic equation for $|f_i(\omega)|^2$, where $f_i(\omega)$ can be obtained using Eq. (12), is not particularly demanding, but the outcome may turn out to be puzzling, with three real solutions. These are the cases where optical bistability and hysteresis occur.[28] The optical bistability was studied earlier for a metal particle[35] and nanoshells[36] using another representation for $\chi^{(3)}$. As shown in Fig. 4, for Ag, with the dielectric functions given by Eqs. (6) and (7), we encounter such behavior, which is accompanied by the convergence problem for 'larger' particles with $R \geqslant 4$ nm.

IV. CONVERGENCE CRITERION AND THE BROYDEN METHOD

Once the nonlinear CDE has been obtained, it has to be solved. We approach this by assuming a finite number of scattering events in each iteration, similar to the approach by Hill *et al.*[18] The initial step involves calculations of the polarizability, with a given incident field having uniform distribution throughout the fractal. The self-consistent cycle is then started and repeated until the convergence is achieved (see Fig. 3).

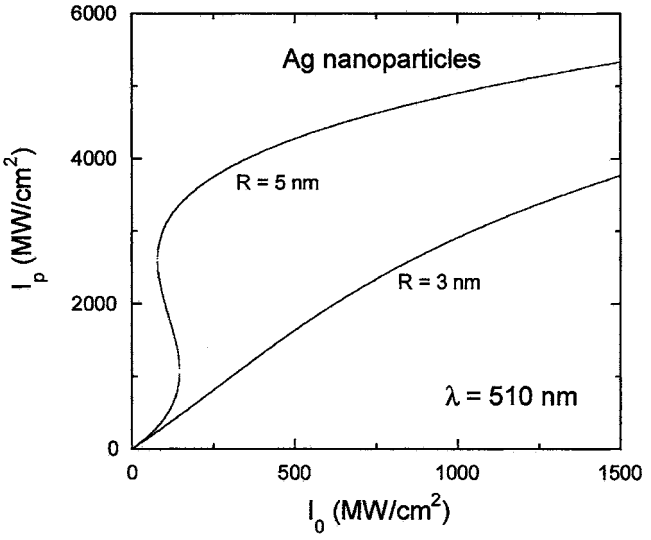

FIG. 4. Optical bistability in 5-nm Ag particles at $\lambda=510$ nm. For comparison, we include results for 3-nm particles that do not exhibit an optical bistability.

In order to deduce whether our results are converged, we use the following error percentage:

$$\varepsilon(\%) = 100\frac{|G^{(k)} - G^{(k-1)}|}{G^{(k)}} = 100\frac{|\mathbf{E}^{(k)} \cdot (\mathbf{E}^{(k)})^* - \mathbf{E}^{(k-1)} \cdot (\mathbf{E}^{(k-1)})^*|}{\mathbf{E}^{(k)} \cdot (\mathbf{E}^{(k)})^*}, \tag{21}$$

where the $\mathbf{E}^{(k)} \cdot (\mathbf{E}^{(k)})^*$ is the dot product of the $3N$-dimensional local-field vectors at the kth iteration. In our case, we chose $\varepsilon(\%) \leqslant 1\%$ for three-dimensional fractals, while in our two-dimensional systems, $\varepsilon(\%) \leqslant 0.01\%$. Time consumption was the main consideration for choosing a larger value for $\varepsilon(\%)$ in the case of three-dimensional fractals. The values above were taken as the convergence criteria for the two systems.

Without further manipulation, a direct solution of the CDE is usually not possible, because it would strongly oscillate between different states, preventing convergence from occurring. The problem lies in the fact that there is no damping for oscillations between successive iterations, a quite common problem in self-consistent field calculations. In the case when there is a single unique solution, it is possible to introduce a damping term by using a linear combination of the resulting parameters for adjacent iterations, and applying this for modification of the input parameters in the upcoming iteration. This method is referred to as simple "linear mixing," but it does not work in the case of nonunique solutions, which is the case for our fractal system consisting of 5-nm particles, where we have a "weak" hysteretic behavior.

Therefore, we have to explore other "mixing" schemes. The Broyden method uses "mixing" of all resulting quantities; in our case the internal field intensities for each monomer:

$$I_p^{(k+1)} = I_p^{(k)} - [J^{(k)}]^{-1} F(I_p^{(k)}), \tag{22}$$

where $J^{(k)}$ is a Jacobian matrix and $F(I_p^{(k)})$ is defined by the self-consistency condition using a Kohn-Sham type variational principle.[37] Using Eq. (22), the "effective" mixing is determined by updating the Jacobian matrix $J^{(k)}$ between successive iterations starting from a good initial guess, referred to as the Newton-Raphson (Jacobian update) method.[38] The Broyden method has been modified by D.D. Johnson,[39] and the modified Broyden method is now widely used in quantum chemistry to perform first-principles electronic-structure calculations. The modified Broyden method is more general and can be applied to a broad class of other problems, and we have utilized it for our purpose. Compared to the updating procedure in the regular Broyden method, the modified Broyden method incorporates information from all previous iterations, and all of this information is used in the update of the Jacobian matrix (described in detail in Ref. 38). The modified Broyden method is more efficient in terms of memory storage and convergence behavior. As mentioned above, for fractals consisting of particles with $R > 4$ nm, we find that a hysteretic behavior develops in a certain spectral range. Therefore, it is necessary to keep track of the history of roots for the solution and the branch to follow for each particle in the fractal. Using the modified Broyden method, we found that we can achieve convergence for the case of weak hysteretic behavior (as observed for fractals of 5-nm particles). The convergence for larger particles remains a problem. Therefore, we limit our calculations to fractals consisting of monodisperse nanosized Ag particles of $R=3$ nm, where $f(\omega)$ converges to a single-valued function at all investigated intensities, and $R=5$ nm, where we observe a weak hysteretic behavior (see Fig. 4).

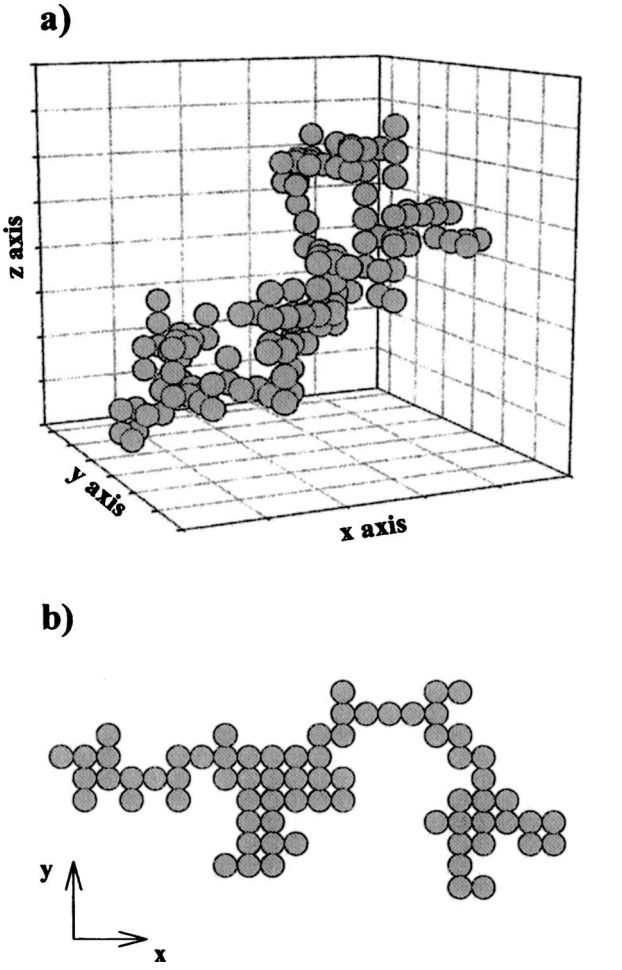

FIG. 5. A typical three-dimensional fractal aggregate consisting of 130 nanosized Ag particles and its projection onto the *xy* plane.

V. RESULTS AND DISCUSSION

Because of computational time limitations (the calculations were done on a PC), we considered three-dimensional fractal aggregates consisting of 130 monomers of the two radii mentioned above. We assumed equal particle size for all particles in the aggregates because it is simpler to extract the relevant features and it allows us to study the properties of the aggregates compared with the properties of single particles of the size. Generally, fractal aggregates will consist of particles with some size distribution, and this will lead to inhomogeneous broadening of the absorption spectra.[40] A typical fractal aggregate used in our simulations is shown in Fig. 5. We are mainly interested in general properties of such fractal aggregates rather than in features caused by the specific arrangement of particles in any particular fractal. Thus, using the random walk model, we produced about 20 different fractal aggregates embedded in the three-dimensional space, and used ten different light polarizations for each of those aggregates. The results were averaged over all these aggregates and polarizations.

With the methods outlined above, we were able to compute the enhancement factors for fractals consisting of 3- and 5-nm particles for the intensities close to 0.0001, 15, and 58 MW/cm^2. It should be noted that in our model we considered the Kerr nonlinear susceptibility $\chi^{(3)}$. In order to safely neglect contributions due to higher-order terms, our calculations are limited to lower incident intensities (up to 60 MW/cm^2) and wavelengths (up to 1500 nm) to ensure that the calculations are governed by the condition[41]

$$\frac{G^{(k)} I_0}{I_s} < 1. \tag{23}$$

Here, $G^{(k)}$ is the average enhancement in the fractal at the kth iteration, and the saturation intensity I_s is given by

$$I_s^{-1} = \frac{2}{15}\left(\frac{eR}{\hbar\omega}\right)^2 \frac{\Gamma_2}{\Gamma_1}. \tag{24}$$

Figures 6(a) and 6(b) display the computed average enhancement $G^{(N)}$ as a function of wavelength using three different incident intensities for $R=3$ nm and $R=5$ nm, respectively. $G^{(N)}$ denotes the converged result [cf. Eq. (18)] after N iterations. For comparison, we have included the average enhancements for single particles at 0.0001 and 58 MW/cm^2. As we pointed out in Ref. 28, individual particles exhibit a single resonance with a well-defined dependence on the incident field, and its properties are solely determined by the dielectric properties, the particle size of the material and its

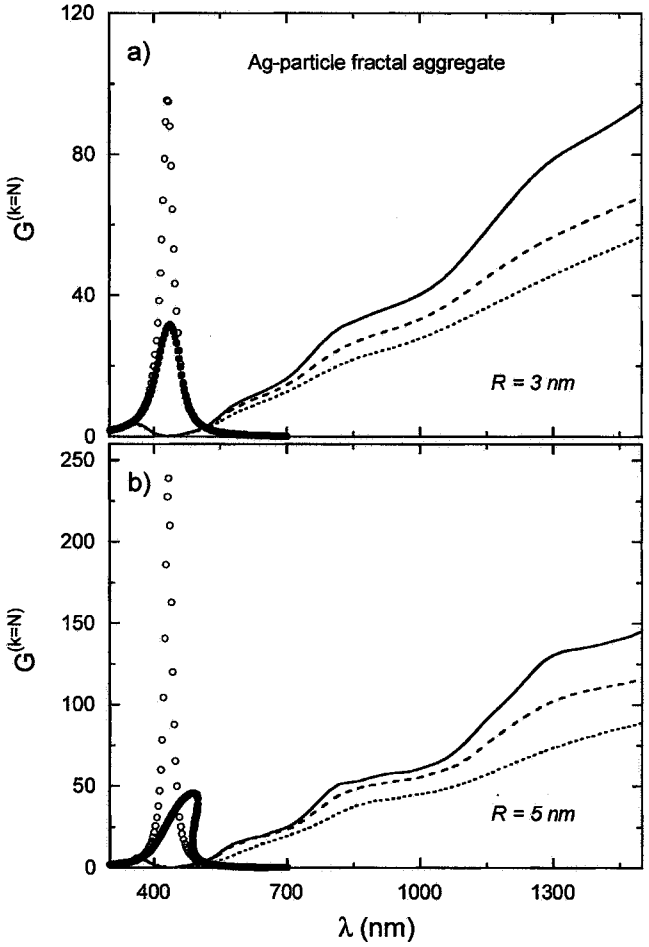

FIG. 6. Wavelength dependence of the average enhancement factor at three incident intensities 0.0001 (thick line), 15 (dashed line), and 58 (thin line) MW/cm^2 for fractals consisting of 130 Ag monomers of (a) R=3 nm and (b) R=5 nm. For comparison, we include the enhancement factors for individual particles at 0.0001 (open symbols) and 58 (closed symbols) MW/cm^2.

surroundings. Unlike individual particles, the properties of fractal aggregates are determined by collective effects of the aggregate.

At higher wavelengths, fractal aggregates of both particle sizes exhibit a tendency toward a more linear behavior and the suppression of the step-like feature in for the average enhancement as a function of intensity. Our results are consistent with the notion that the individual resonances of a fractal aggregate are suppressed because of saturation effects.

Figure 7 shows the average enhancement for 5-nm-particle fractals as a function of the wavelength and incident intensity in form of a color-density plot. It can be seen that the sharp steps at low incident intensities shift to slightly higher wavelengths and experience suppression with an increase of the incident intensity. At the highest intensities, an almost continuous increase in the wavelength dependence of the enhancement factor is found.

The determination of the average enhancement factor in fractal aggregates is of little use to experimentalists, as this property normally is not measured directly. However, using

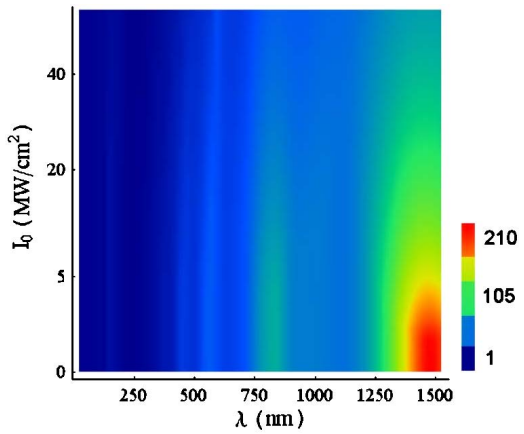

FIG. 7. (Color online) Intensity and wavelength dependencies of the average enhancement factor for fractal consisting of 5-nm Ag particles.

the same procedure introduced above, it is possible to calculate the optical extinction cross-section spectra, which is an experimentally observable quantity. The extinction cross section is given by[42]

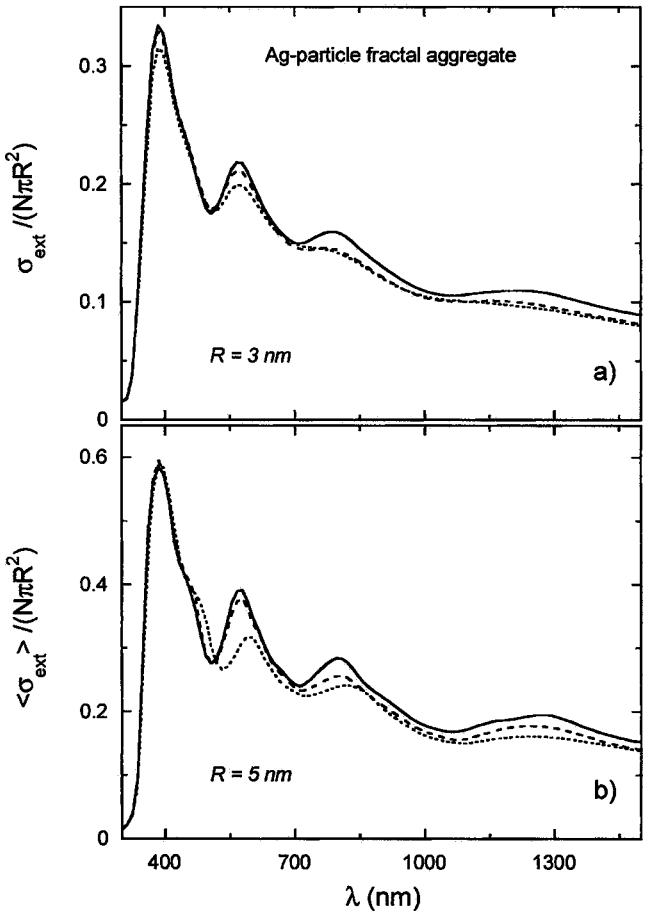

FIG. 8. Spectra of the extinction cross section at three incident intensities 0.0001 (thick line), 15 (dashed line), and (thin line) 58 MW/cm^2 for fractal aggregates consisting of 130 Ag monomers of (a) R=3 nm and (b) R=5 nm. The cross section is normalized per area of N particles.

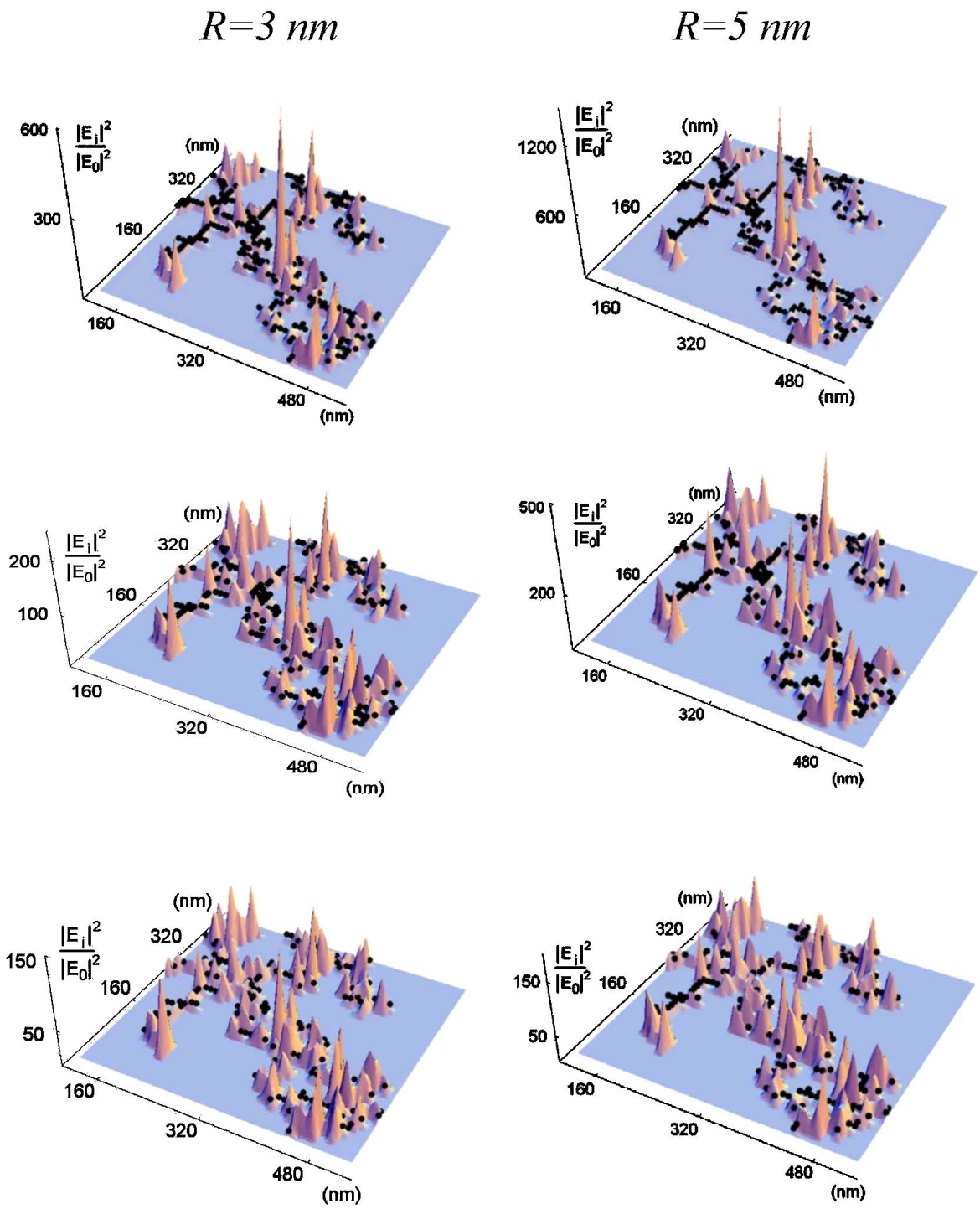

FIG. 9. (Color online) Spatial distribution of the local field intensity factors for two-dimensional fractals consisting of 500 Ag monomers at three different intensities for 3-nm aggregates (left) and 5-nm aggregates (right) at $\lambda = 805$ nm. The upper panel displays the results for the incident energy of 0.0001, the middle panel at 15, and the bottom panel at 58 MW/cm^2. Note, the scales of the vertical axis are different.

$$\langle \sigma_e \rangle = \frac{4\pi k}{|E_0|^2} \langle \mathrm{Im}(\mathbf{E}^0 \cdot \mathbf{d}) \rangle, \tag{25}$$

where $\langle \sigma_e \rangle$ denotes the average over all possible polarizations and different clusters, k is the modulus of the wave vector and $(\mathbf{E}^0 \cdot \mathbf{d})$ represents the dot product of the incident field $\mathbf{E}^0$ and the resulting dipole moment $\mathbf{d}$.

The calculated extinction cross sections for 3-nm- and 5-nm-particle fractals are shown in Figs. 8(a) and 8(b) respectively. We find that the calculated extinction cross sections reflect the predicted changes for the average enhancement factor and its intensity dependence. The differences between the curves are large enough to be resolved experimentally. In addition, we find a moderate (but noticeable)

shift for the first minimum toward higher wavelengths with increasing intensity for fractals consisting of 5-nm monomers, a feature that is not observed for 3-nm-particle fractals. This shift is due to a change in the resonance condition (weak hysteretic behavior) of the denominator,

$$\varepsilon_{0m} + 12\pi\chi^{(3)}|f_i(\omega)|^2 I_{i,local} + 2\varepsilon_h \cong 0,$$

in Eq. (9).

Finally, we studied the spatial distribution of the local intensities in fractal aggregates. For the sake of clarity of the presentation, we computed the spatial distributions for one particular two-dimensional fractal, consisting of 500 Ag monomers with radii of 3 and 5 nm, at the three different intensities. The results are shown in Fig. 9. At low incident intensity, we find very similar spatial distributions for fractal aggregates with the two particle sizes. Both fractals exhibit large enhancement of the local field intensities, which are localized within a few distinct areas of the fractal, the so-called *hot spots*. The reduced enhancement in the 3-nm fractals compared to the 5-nm ones can be attributed to the smaller dipole moments of the 3-nm particles. With increasing intensity, however, the differences become apparent between the 3-nm- and 5-nm-particle fractals. It can be seen that the peak intensities of the *hot spots* are suppressed much faster for the larger 5-nm-particle fractals. In particular, we find that the largest enhancement is reduced by a factor of ~3 for the 3-nm aggregate, while it is reduced by a factor of ~10 for the 5-nm aggregate. The overall behavior of the local field distribution with increasing incident intensity follows some intuitively anticipated behavior, with the highest peaks suppressed first such that a more uniform spatial distribution is found at higher intensities. We may also compare the enhancement of particle aggregates with the one for a single particle (see Fig. 4). At very low incident intensities, the local-field enhancement, $|E_{i,peak}|^2/|E_0|^2$, for the 5-nm-particle aggregate in Fig. 9 is more than 5 times larger than the single-particle one. This is due to the fact that many surrounding particles contribute to a particular hot spot.

Particular sites, which in this case could be called *cold spots*, have also shown up in our test of the quasistatic approximation. As mentioned in the introduction, introducing the terms of order kr_{ij} and $(kr_{ij})^2$ into the interaction matrix and maintaining the exponential factors in Eq. (3) does not affect the calculated average enhancement significantly. However, if one looks at the results for particular monomers before averaging over the polarization vectors, the difference between intensities calculated with Eqs. (5) and (6) are noticeable: for an aggregate of 130 monomers a few percentage points on average and more than 100% in exceptional cases. Such exceptional sites are the cool spots, where the quasistatic approximation gives a very small intensity. Evidently, at cool spots the near-field contributions from other monomers nearly cancel and the far fields happen to add up constructively. This picture is confirmed by the fact that the role of the terms beyond the quasistatic approximation increases with the size of the aggregates. For 500 monomers, which form an aggregate of linear dimension exceeding 700 nm, we find that the difference between the two approaches is about 10% on average and at cold spots it can be more than an order of magnitude.

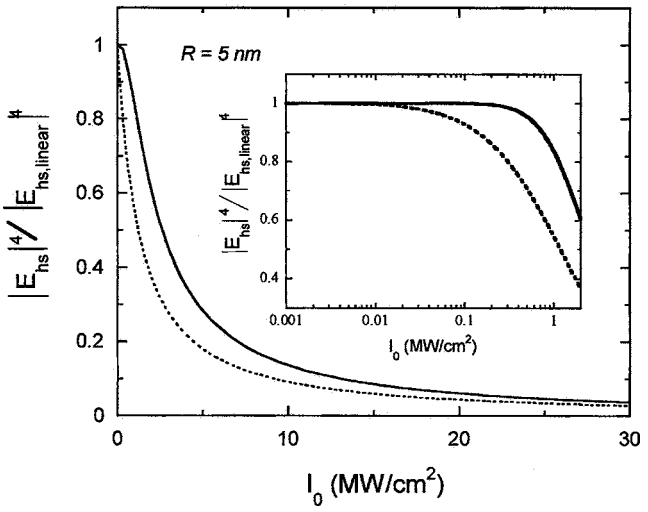

FIG. 10. Intensity dependence of SERS signal enhancement normalized to its linear (low intensity) value. The thick line represents the response of a single 5-nm particle at $\lambda = 420$ nm, and the dotted line represents the peak value in the spatial distribution for a fractal consisting of 5 nm particles at $\lambda = 1260$ nm. The insert shows the same on a semi-logarithmic scale.

Next, we have investigated the saturation effects in fractal aggregates in comparison with the single particles. Figure 10 shows the local SERS enhancement for a single particle compared with a fractal aggregate consisting of particles of that size. The SERS signal is proportional to the square of the local intensity enhancement,[43] and it is considered here because of its particular importance in the case of single-molecule detection. It can be seen that the saturation effects are stronger in fractals compared to single particles, but not as much as one could expect. This again emphasizes that the contributions to a hot spot come from all surrounding particles, in other words, the enhancement effects in fractal aggregates are due to collective effects. In the insert of Fig. 10, we show the intensity dependence of the SERS enhancement on a logarithmic scale. The most striking feature is that nonlinear effects set in at much lower incident intensities for the fractal aggregates as opposed to the single particles. The exact value for an "upper boundary" to the linear behavior depends on many parameters (e.g., fractal size and realization, incident wave polarization, wavelength, and others). However, from our particular example used in Fig. 10, it is apparent that nonlinear effects may become dominant at intensities well below the ones in typical SERS experiments, and that they should not be neglected.

VI. CONCLUSIONS

Motivated by the unlikely magnitude of dipole moments calculated in the linear approximation for certain sites in fractal aggregates, we have undertaken to include the third-order polarizability in the calculation of the effect of high-intensity electromagnetic waves. As expected, this correction reduces the predicted enhancement of the incident field in the

monomers comprising the aggregate. In particular, under an incident intensity of 58 MW/cm^2, the giant enhancements found at *hot spots* are reduced by a factor of 3 to 10 with respect to the linear case.

For comparison with experimental results, one needs to average over the orientation of the electric field with respect to the cluster and over a large number of clusters. The effect of the nonlinear term in the polarizability on such averages is not spectacular; the reduction is less than 40% in the largest field where higher than third-order corrections are not important. On the other hand, to understand some of the nuances, it is useful to study the results of calculations on particular clusters with particular orientations of the field. A close look at Fig. 9 reveals that the saturation tendency due to the third-order correction to the linear polarizability is by no means uniform. In particular, we can observe that in the aggregate of 5-nm particles the largest enhancement occurs at different sites for different intensities. The overall effect is one of leveling: at the strongest external field, we see many peaks of approximately the same enhancement.

In summary, we have shown that saturation effects decrease the local field factors and provide a basic limitation for the intensity of the electromagnetic field that can be created inside the particle. It should be noted that the model aggregates employed for our calculations yield only relatively moderate enhancement factors. As we mentioned above, the local enhancements in real fractal aggregates may be as high as 10^5, and therefore saturation effects may become important at even lower incident intensities. These details deserve further study, including the phase of the signal at different sites.

ACKNOWLEDGMENT

The authors thank E. Fernandez for help with several of the diagrams and figures. This work was supported in part by NSF awards DMR-0121814, 0210445-ECS, and HRD-0317722, and NASA award NCC3-1035.

*Electronic mail: abuin@nmsu.edu

[1] U. Kreibig and M. Vollmer, *Optical Properties of Metal Clusters* (Springer Verlag, Berlin, 1995).
[2] V. M. Shalaev, *Nonlinear Optics of Random Media: Fractal Composites and Metal-Dielectric Films* (Springer Verlag, Heidelberg, 2000).
[3] M. I. Stockman, in *Optics of Nanostructured Materials*, edited by V. A. Markel and T. F. George (Wiley, New York, 2000), pp. 313–353.
[4] V. A. Markel, V. M. Shalaev, and T. F. George, in *Optics of Nanostructured Materials*, edited by V. A. Markel and T. F. George (Wiley, New York, 2000), pp. 355–412.
[5] M. Moskovits, Rev. Mod. Phys. **57**, 783 (1985).
[6] G. C. Schatz and R. P. Van Duyne, in *Handbook of Vibrational Spectroscopy*, edited by J. M. Chalmers and R. P. Griffiths (Wiley, New York, 2002), pp. 759–774.
[7] K. Kneipp, Y. Wang, H. Kneipp, L. T. Perelman, I. Itzkan, R. R. Dasari, and M. S. Feld, Phys. Rev. Lett. **78**, 1667 (1997).
[8] H. Xu, E. J. Bjerneld, M. Kall, and L. Borjesson, Phys. Rev. Lett. **83**, 4357 (1999).
[9] H. Xu, J. Aizpurua, M. Kall, and P. Apell, Phys. Rev. E **62**, 4318 (2000).
[10] M. I. Stockman, S. V. Faleev, and D. J. Bergman, Phys. Rev. Lett. **88**, 067402-1 (2002).
[11] B. M. Smirnov, *Physics of the Fractal Clusters* (Nauka, Moscow, 1991).
[12] R. Jullien and R. Botet, *Aggregation and Fractal Aggregates* (World Scientific, Singapore, 1987).
[13] V. P. Drachev, S. V. Perminov, S. G. Rautian, V. P. Safonov, and E. N. Khaliullin, JETP **94**, 901 (2002).
[14] V. P. Drachev, S. V. Perminov, S. G. Rautian, and V. P. Safonov, JETP Lett. **68**, 651 (1998).
[15] J. M. Gerardy and M. Ausloos, Phys. Rev. B **25**, 4204 (1982).
[16] M. Quinten, Appl. Phys. B: Lasers Opt. **73**, 245 (2001).
[17] S. A. Maier, P. G. Kik, and H. A. Atwater, Phys. Rev. B **67**, 205402 (2003).
[18] S. C. Hill, G. Videen, W. Sun, and Q. Fu, Appl. Opt. **40**, 5487 (2001).
[19] E. M. Purcell and C. R. Pennypacker, Astrophys. J. **186**, 705 (1973).
[20] A. A. Lazaridies and G. C. Schatz, J. Phys. Chem. B **104**, 460 (2000).
[21] J. A. Stratton, *Electromagnetic Theory* (McGraw-Hill, New York, 1941).
[22] V. A. Markel, L. S. Muratov, M. I. Stockman, and T. F. George, Phys. Rev. B **43**, 8183 (1991).
[23] Yu. E. Danilova, V. A. Markel, and V. P. Safonov, Atmos. Oceanic Opt. **6**, 1436 (1993).
[24] V. A. Markel, V. N. Pustovit, S. V. Karpov, A. V. Obuschenko, V. S. Gerasimov, and I. L. Isaev, Phys. Rev. B **70**, 054202 (2004).
[25] V. A. Markel, V. M. Shalaev, E. B. Stechel, W. Kim, and R. L. Armstrong, Phys. Rev. B **53**, 2425 (1996).
[26] S. G. Rautian, JETP **85**, 451 (1997).
[27] F. Hache, D. Ricard, and C. Flytzanis, J. Opt. Soc. Am. B **3**, 1647 (1986).
[28] V. P. Drachev, A. K. Buin, H. Nakotte, and V. M. Shalaev, Nano Lett. **4**, 1535 (2004).
[29] K. Uchida, S. Kaneko, S. Omi, C. Hata, H. Tanji, Y. Asahara, and A. J. Ikushima, J. Opt. Soc. Am. B **11**, 1236 (1994).
[30] V. P. Drachev, E. N. Khaliullin, W. Kim, F. Alzoubi, S. G. Rautian, V. P. Safonov, R. L. Armstrong, and V. M. Shalaev, Phys. Rev. B **69**, 035318 (2004).
[31] N. Bloembergen, *Nonlinear Optics* (World Scientific, River Edge, Singapore, 1996).
[32] While the values for g_1 and g_3 reported in Ref. 23 are correct, for the determination of the enhancement factors in Figs. 4–6 in the same reference, we mistakenly used $g_1=g_3=1$. As a consequence, the absolute values shown in that figure are approximately 30% too low, while the qualitative behavior was not jeopardized.

[33] G. P. Ortiz and W. L. Mochan, Phys. Rev. B **67**, 184204 (2003).
[34] *Numerical Recipes in Fortran 77*, edited by W. H. Press, S. A. Teukolvsky, W. T. Vetterling, and B. P. Flannery (University Press, Cambridge, 2001).
[35] Y. K. Yoon, R. S. Bennink, R. W. Boyd, and J. E. Sipe, Opt. Commun. **179**, 577 (2000); J. W. Haus, N. Kalyaniwalla, R. Inguva, and C. M. Bowden, J. Appl. Phys. **65**, 1420 (1989).
[36] N. Kalyaniwalla, J. W. Haus, R. Inguva, and M. H. Birnboim, Phys. Rev. A **42**, 5613 (1990).
[37] W. Kohn and L. J. Sham, Phys. Rev. **140**, 1133 (1965); P. Bendt and A. Zunger, Phys. Rev. B **26**, 3114 (1982).
[38] G. P. Srivastava, J. Phys. A **17**, L317 (1984).
[39] D. D. Johnson, Phys. Rev. B **38**, 12807 (1988).
[40] S. V. Perminov, S. G. Rautian, and V. P. Safonov, JETP **98**, 691 (2004).
[41] Strictly speaking, the criterion formulated in Eq. (20) is not completely correct, but the requirement should be imposed on each site in each fractal considering the local enhancement at that site. For our case, it turns out that using above criterion is relatively safe and only very few particles (2–3 particles) located at *hot spots* slightly exceed unity.
[42] V. A. Markel, J. Opt. Soc. Am. B **12**, 1783 (1995).
[43] J. Gersten and A. Nitzan, J. Chem. Phys. **73**, 3023 (1980).